ChemSusChem

Research Article
doi.org/10.1002/cssc.202301801

Chemistry Europe
European Chemical Societies Publishing

www.chemsuschem.org

Repurposing Kraft black Liquor as Reductant for Enhanced Lithium-Ion Battery Leaching

Ana R. F. Carreira,[a] André F. M. Nogueira,[a] Inês L. D. Rocha,[a] Filipe Sosa,[a] André M. da Costa Lopes,[a, b] Helena Passos,[a, c, d] Nicolas Schaeffer,*[a] and João A. P. Coutinho[a]

The economic advantages of H_2SO_4 make it the acid of choice for the hydrometallurgical treatment of waste lithium-ion batteries (LIBs). However, to facilitate the full dissolution of the higher valency metal oxides present in the cathode black mass, a suitable reducing agent is required. Herein, the application of industrial black liquor (BL) obtained from the Kraft pulping for papermaking is investigated as a renewable reducing agent for the enhanced leaching of transition metals from LIB powder with H_2SO_4. The addition of acidified BL to H_2SO_4 significantly improved the leaching efficiency for a range of LIB cathode chemistries, with the strongest effect observed for manganese-rich active material. Focusing on NMC_{111} ($LiMn_xCo_yNi_zO_2$) material, a linear correlation between the BL concentration and the leaching yield of Mn was obtained, with the best overall leaching efficiencies being achieved for 2.0 mol L^{-1} H_2SO_4 and 50 vol% of BL at 353 K. A quasi-total degradation of oxygenated and aromatic groups from the BL during NMC_{111} dissolution was observed after leaching, suggesting that these chemical groups are essential for LIB reduction. Finally, the leached transition metals could be easily recovered by pH adjustment and oxalic acid addition, closing the resource loop and fostering resource efficiency.

Introduction

Lithium-ion batteries (LIBs) have emerged as vital drivers of the clean energy revolution, powering electric vehicles, portable electronic devices and storing renewable energy in grid systems.[1] The widespread adoption of LIBs is attributed to their unique features, such as high energy density, high voltage, high capacity and high stability, acknowledged by the 2019 Nobel Prize in chemistry.[2,3] However, efficient battery waste management and their sustainable recycling are still catching-up with the range of end-of-life battery compositions and volume.[4] The varying lifespan of LIBs in different applications (≈2 years cell phones, ≈3–4 years consumer electronics and >10 years for electric vehicles), LIB cell heterogeneity and the complexity inherent to the multiple LIB chemistries (LCO, LMO, LMNO, NMC, LFP) hinder the development of efficient recycling strategies.[5] By 2030, around 11 million metric tons of LIBs are forecast to reach their end-of-life, leading to a surging and concerning issue of spent LIB accumulation.[6] Correspondingly, the global LIB recycling market is estimated to reach 21.7 billion € by 2030, representing more than a thirteen-fold increase between 2017 and 2030 and suggesting an appealing opportunity for metal recovery.[7] Spent LIBs can be harnessed into valuable secondary resources, with cathode constituents accounting for ≈30% of the LIB manufacturing cost.[8] The manufacture of LIBs requires several elements, such as cobalt, lithium, manganese, graphite, copper and nickel, which are classified as critical raw materials by the EU due to their supply risk and/or economic importance.[9]

Urban mining can alleviate the unprecedented pressure on primary ores while securing a circular supply chain and fostering environmental benefits. The endorsement of more sustainable practices for the recycling and repurposing of LIBs through EU legislation is fueling the pursuit of efficient and greener LIB recycling processes.[10] The recycling of LIBs can be accomplished by hydrometallurgy, pyrometallurgy or direct recycling.[8,11] Pyrometallurgy and hydrometallurgy are implemented at an industrial level. However, current recycling practices based on pyrometallurgy result in lower recovery rates and product quality as well as a higher carbon footprint relative to hydrometallurgical approaches. Hydrometallurgy encompasses metal leaching, separation, and purification. Conventional hydrometallurgy often relies on multi-step treatments and uses concentrated inorganic acids (HCl, HNO_3 and H_2SO_4) as leaching media, resulting in gaseous emissions and large volumes of wastewater.[1] Over the past decade, significant

[a] A. R. F. Carreira, A. F. M. Nogueira, I. L. D. Rocha, F. Sosa, A. M. da Costa Lopes, H. Passos, N. Schaeffer, J. A. P. Coutinho
CICECO – Aveiro Institute of Materials, Department of Chemistry, University of Aveiro, 3810-193 Aveiro, Portugal
E-mail: nicolas.schaeffer@ua.pt

[b] A. M. da Costa Lopes
CECOLAB – Collaborative Laboratory Towards Circular Economy, R. Nossa Senhora da Conceição, 3405-155 Oliveira do Hospital, Portugal

[c] H. Passos
LSRE-LCM – Laboratory of Separation and Reaction Engineering – Laboratory of Catalysis and Materials, Faculty of Engineering, University of Porto, Rua Dr. Roberto Frias, 4200-465 Porto, Portugal

[d] H. Passos
ALiCE – Associate Laboratory in Chemical Engineering, Faculty of Engineering, University of Porto, Rua Dr. Roberto Frias, 4200-465 Porto, Portugal

Supporting information for this article is available on the WWW under https://doi.org/10.1002/cssc.202301801

efforts have been made to develop suitable and green leaching media to achieve high recycling efficiencies while minimizing the environmental footprint of this process. Counterintuitively, the use of bio-derived leaching agents based on common organic acids such as formic, lactic, or citric acids yield a larger environmental impact compared to cheaper inorganic acids like H_2SO_4 due to the carbon footprint and cost associated with their production.[12] However, to facilitate the full dissolution of the more recalcitrant higher valency metal oxides present in the cathode black mass, the latter must be paired with a suitable reducing agent to ensure the reduction of the transition metals present and improve the leaching intensification.[13]

Pairing milder lixiviants with H_2O_2 is an extensively used combination, but the explosive nature and chemical instability of this reducing agent pose some safety concerns.[14–16] The employment of green reductants is usually associated with monosaccharides (D-glucose) and ethanol.[17,18] Recently, biomass wastes have been proposed as eco-friendly, bioavailable and low-cost reductants for the efficient recovery of metals from spent LIBs.[19–22] Using biomass wastes, such as tea waste, orange peels and grape seeds, offers a promising avenue for metal dissolution due to their rich composition of reactive molecules. These wastes contain a wide array of compounds, including polyphenols, phenolic acids, saccharides, cellulose, and hemicellulose, which exhibit notable reductive properties. Under acidic conditions, the breakdown of lignocellulosic content affords oligo- and monosaccharides, such as glucose, fructose, xylose, and arabinose.[23] These saccharides contain hydroxyl groups that can act as effective green reductants in the redox-based metal dissolution. Despite the promise of the waste-to-wealth concept, few works exploit the reducing power of wastes for leaching spent LIBs.[24]

Furthermore, most studies employing green reducing agents use pure biomolecules,[18] which require refinement and purification, or food waste residues that necessitate prior maceration and extraction of the bio-active compounds.[25] These additional steps entail an energetic and financial cost towards their applicability. Therefore, using biological wastes with low refinement from well-established industries could be a more economic, circular, and better resource management approach to achieve the desired goal.

Around 180 million tons of pulp is manufactured annually for paper products, three quarters arising from chemical pulping processes.[26] Among the chemical pulping process, the Kraft process is the most widely adopted, accounting for 75% of the global industry.[27] Kraft pulping involves cooking wood chips in a solution of NaOH and Na_2S, also referred to as white liquor, to separate lignin from cellulose fibers. During the cooking process, lignin-lignin and lignin-polysaccharide bonds are partially cleaved, enabling lignin dissolution in alkaline pH and forming a dark and viscous liquid known as black liquor (BL). After this process, nearly 7 tons of BL are generated *per* ton of pulp production.[28] Depending on the raw material composition, the resulting BL contains dissolved lignin, hemicelluloses, minor amount of cellulose, their degradation products (e.g. aliphatic and hydroxylated carboxylic acids, phenolic and non-phenolic aromatic compounds, furans, among others), and inorganic compounds (e.g. NaOH, Na_2S, $NaCO_3$, Na_2SO_3, among others).[26,27] Lignin has been applied as an efficient reductant for pyrolusite, whereas hemicellulose and cellulose-rich sawdust have been successfully employed as green reductants in the leaching of manganese ores.[29,30] Annually, an estimated 1.3 billion tons of BL is produced. The main valorization route of this byproduct is through its combustion in a recovery boiler, producing around 700 million tons of steam and generating energy to power various parts of the production plant. The energy recovered from combustion is often excessive, prompting the pulping industry to investigate other chemical recovery pathways.[28,31] This work proposes a novel and green waste for waste circular approach by harnessing the redox power of BL for metal leaching from cathode powder in a diluted H_2SO_4 medium.

Experimental

Materials

Cathode powder NMC_{111} ($LiNi_{0.33}Mn_{0.33}Co_{0.33}O_2$, >98 wt%), LMNO ($LiMn_{1.5}Ni_{0.5}O_4$, >98 wt%), LMO ($LiMn_2O_4$, >99 wt%), nickel(II) oxide (99 wt%), vanillin (99 wt%), yttrium standard (1000 mg L^{-1} of Y(III) in 2 wt% nitric acid) and poly(vinyl alcohol) (>99 wt%) were acquired from Sigma Aldrich. LCO ($LiCoO_2$, 99.5 wt%), cobalt(II) oxide (95 wt %) and oxalic acid (98 wt%) were acquired at Alfa Aesar. Lithium hydroxide anhydrous (>98 wt%) was purchased from TCI. Hydrochloric acid (37 wt%) was purchased from Honeywell. Lithium chloride (99 wt%), magnesium sulfate·heptahydrate (>99 wt%), gallic acid (99.5 wt%) and Folin-Ciocalteu reagent (2 M with respect to acid) were purchased from Merck. Sulfuric acid (95 wt%), ethanol (analytical reagent grade), methanol (99.9 wt%), acetic acid glacial (analytical reagent grade) and D-Glucose (99 wt%) were acquired from Fischer Scientific. Sodium carbonate anhydrous (99.9 wt%), sodium thiosulphate anhydrous (99 wt%) and iron sulfate (III) heptahydrated (analytical reagent grade) and formic acid were purchased from Prolabo, Panreac and Carlo Erba, respectively. Ammonia solution 25 vol% was acquired from Labkem. Double distilled water was obtained through a Millipore filter system MilliQ® at room temperature. The Navigator Company (Portugal) kindly provided the BL sample, which was stored in the refrigerator at ≈277 K. For HPLC analysis, methanol and formic acid were purchased from Fischer Scientific (HPLC grade) and Carlo Erba (purity ≥99%), respectively. Syringe filters (0.45 μm pore size; Specanalitica) and membrane filters (0.22 μm; Sartorius Stedim Biotech) were applied in filtration steps.

BL pretreatment and characterization

Due to the alkaline nature of the as-received BL (pH ~14), an acidification step using H_2SO_4 (95 wt%) was included as pre-treatment prior to its use in all leaching experiments. This was done to prevent the precipitation of lignin whilst also avoiding any acid neutralization effect upon mixing with additional H_2SO_4 during the leaching reaction. The acidification of BL was performed in two stages through the dropwise addition of concentrated H_2SO_4. At pH = 6.0, a considerable amount of precipitate was observed in the BL in accordance with previous reports due to the decreased ionization of lignin functional groups and increased agglomeration.[32] After 1 h of mixing at pH = 6.0, the precipitate was removed through filtration, and the BL was further acidified until pH = 2.0, filtered and stored at 277 K prior to use. The pH of

the BL was controlled using a Mettler Toledo SevenMultiTMdual pH meter (±0.02) and all filtrations were carried out using a 0.45 μm pore size syringe filter.

The total phenolic content of the treated BL was determined according to the method of Bonoli *et al*[33] by colorimetry using the Folin-Ciocalteu reagent (a mixture of sodium tungstate and phosphomolybdic acid in phosphoric acid along with lithium sulfate and bromine). The method relies on an electron-transfer reaction between a reducing species and the Folin-Ciocalteu reagent (oxidant). The reduction of the phosphotungstic and phosphomolybdic anionic derivatives by phenolic compounds causes a from yellow to blue. The magnitude of the final color shift is directly proportional to the reducing activity of the phenolic compounds.[34] Briefly, 100 μL of the BL was homogenized for 1 min with 500 μL of Folin-Ciocalteu reagent and 6 mL of distilled water. Afterwards, 2 mL of 15% Na_2CO_3 was added, and the mixture was homogenized for 0.5 min. Finally, the solution was totaled up to 10 mL with distilled water. After 2 h, the absorbance of the BL was analyzed by UV-spectroscopy using a SHIMADZU UV-1700 Pharma-Spec spectrometer at 750 nm and room temperature in quartz cuvettes. The total phenolic content was determined as gallic acid equivalent (GAE) by plotting the gallic acid calibration curve (from 1 to 1500 $\mu g\,mL^{-1}$). Although the results are expressed in GAE, it is important to note that the Folin-Ciocalteu reagent reacts with any reducing substance and not exclusively phenolic compounds. The results are therefore best understood as a measure of the total reducing capacity of the acidified BL.[34]

The initial composition of acidified BL was determined *via* gas chromatography mass spectroscopy (GC-MS) with prior silylation. A 4 mL aliquot of the acidified BL was dried under vacuum at room temperature until a dried powder was obtained. Approximately 20 mg of dried BL was dissolved in 250 μL of pyridine, 250 μL of N,O-bis(trimethylsilyl)-trifluoroacetamide and 50 μL of trimethylchlorosilane. The mixture was maintained at 343 K for 30 min to promote the reaction. The analysis of samples was performed using a Shimadzu QP2010 Ultra gas chromatograph/mass spectrometer, equipped with an AOC-20i autosampler and a high-resolution quadrupole mass filter. Separation of analytes was performed on a DB-5 ms column (30 m long, 0.25 mm internal diameter and 0.25 μm film thickness) using helium as carrier gas (40 $cm\,s^{-1}$). The chromatographic conditions were as follows: isothermal at 353 K for 5 min, incremental temperature increase from 353 to 523 K (8 K min^{-1}), further increase from 523 to 573 K (4 K min^{-1}) followed by an isothermal period of 5 min at 573 K. The injector temperature was maintained at 593 K and a split ratio of 1:10 was adopted. The MS was operated in electron impact mode with an impact energy of 70 eV. Data was collected at 1 s intervals for a range of m/z 50–1000. The ion source was maintained at 473 K and the interface temperature at 573 K. The relative total intensity (Tr_{int}) of each compound was calculated according to Equation 1:

$$Tr_{int}(\%) = \frac{C_{int}}{T_{int}} \times 100 \quad (1)$$

where C_{int} is the compound peak intensity and T_{int} is the sum of all compound peak intensities.

The aromatic composition of the acidified BL was also followed by high-performance liquid chromatography (HPLC) in the pretreated BL and upon mixing with various aqueous H_2SO_4 solutions before and after LIB leaching. The HPLC was equipped with an analytical C18 reversed-phase column (250×4.6 mm), RP18 CoreShell 5 μm, from SunShell (ChromaNik Technologies, Inc.), and a diode-array detection system (VWR Hitachi Chromaster) operating at 280 nm wavelength. The operating conditions were adapted from Canas *et al.*[35] and comprised an oven temperature of 313 K, a flow rate of 0.8 $mL\,min^{-1}$, an injection volume of 20 μL, and a binary gradient consisting of solvent A, composed of water and formic acid (98:2 v/v), and solvent B, composed of methanol-water-formic acid (70:28:2 v/v), as follows: 90% isocratic A for 5 min, linear gradient from 90 to 30% A for 40 min, 90% isocratic A for 5 min.

The treated BL composition was also followed by FTIR in a PerkinElmer Spectrum BX spectrometer with a diamond crystal and a horizontal Golden Gate attenuated total reflection (ATR) cell. Each sample was analyzed at wavenumbers ranging from 400 to 4000 cm^{-1}, with a resolution of 4 cm^{-1} and a total of 256 scans. The BL, BL + NMC_{111} and BL + NMC_{111} + H_2SO_4 were stirred at 300 rpm for 4 h at (333 ± 1) K and solid:liquid ratio of 25 $g\,L^{-1}$, when applicable. The samples were centrifuged for 5 min at 10 000 rpm and the leachate was freeze-dried with nitrogen gas before analysis to minimize the overlap of water bands.

Metal leaching

Metal leaching was optimized in acidified BL in the presence and absence of additional acid. The influence of the acid selection (H_2SO_4 and HCl), H_2SO_4 acid concentration (from 0.5 to 2.0 $mol\,L^{-1}$), BL volume percent (from 0 to 50 vol%), temperature (313, 333, and 353 K) and kinetics (until 240 min) were evaluated. Unless otherwise stated, standard leaching conditions of 2.0 $mol\,L^{-1}$ H_2SO_4, 50 vol% BL, 333 K, 240 min, and a solid to liquid ratio of 25 $g\,L^{-1}$ were applied with each variable optimized independently whilst keeping all others constant. Additionally, the influence of the LIB battery chemistry was assessed at a fixed solid-to-liquid ratio of 25 $g\,L^{-1}$. Acid stock solutions of 4.0 $mol\,L^{-1}$ H_2SO_4 ($\rho = 1.16\,g\,mL^{-1}$) or 4.0 $mol\,L^{-1}$ HCl ($\rho = 1.07\,g\,mL^{-1}$) were used for all leaching experiments and appropriately diluted to reach the desired acid concentration from 0.5 to 2.0 $mol\,L^{-1}$. All samples were prepared gravimetrically using a Mettler Toledo XP205 analytic balance through the addition of the acid stock solution, acidified BL, and if necessary deionized water to obtain a total leachate volume of 2 mL. The mass fraction of each component was converted to volume percent by correcting for the density; the density of acidified black liquor at 293 K was of 1.09 $g\,mL^{-1}$ as determined using a SVM 3001 Anton Paar viscometer. All leaching experiments were carried out in a custom-made stainless steel sample holder fitted with a PT100 temperature probe with a precision of ±0.1 K and a constant stirring rate of 300 rpm. The probe was previously calibrated against a calibrated platinum resistance thermometer, SPRT100 (Fluke-Hart Scientific 1529 Chub-E4), traceable to the National Institute of Standards and Technology (NIST), with an uncertainty less than 2×10^{-2} K. All reported leaching values represent the average value from three independent experiments.

After leaching, the resulting mixture was centrifuged for 5 min at 10 000 rpm to separate the solid residue from the leachate supernatant. Following the recovery of the supernatant and washing of the solid residue after leaching using deionized water, the latter's composition was followed by powder X-ray diffraction (XRD) using a Bruker AXS with Cu Kα radiation operating at 45 kV and a 396 spinning discs sample holder. The obtained diffractograms were analyzed on the X'pert Highscore Plus software package. The metal content (Co(II), Mn(II) and Ni(II)) in each leachate after centrifugation and filtration using a 0.45 μm pore size filter was quantified by total X-ray fluorescence (TXRF) using a Picofox S2 (Bruker Nano (Billerica, MA, USA)) equipped with a molybdenum X-ray source. The voltage of the X-ray tube was 50 kV and the current 600 μA. The leachate samples were diluted so as to reach a final transition metal concentration between 5 to 25 $mg\,kg^{-1}$ in 1 g of a poly(vinyl alcohol) solution (1 wt%) and spiked with 20 μL of yttrium standard. Prior to analysis, all quartz sample carriers were pretreated with

10 μL of silicon in an isopropanol solution and dried at (353 ± 1) K for at least 15 min. After cooling, 10 μL of each sample was added to a pretreated carrier and subsequently dried on a hot plate at 353 K for a minimum duration of 30 min. The acquisition time for each spectrum was adjusted to 300 s. The quantification of Li(I) was carried out separately using an ion-selective electrode (Mettler Toledo Dx-series, USA). A calibration curve was prepared with LiCl concentrations ranging from 0.1 to 100 mmol L^{-1}. The ionic strength of all standards and samples was buffered using $MgSO_4$. The leaching extraction efficiency (*EE* %) of Li(I), Mn(II), Co(II), and Ni(II) was calculated as shown in Equation 2:

$$EE\ \% = \frac{[M]_{extracted}}{[M]_{total}} \times 100 \quad (2)$$

where $[M]_{extracted}$ is the metal concentration in the leachate (mol L^{-1}) and $[M]_{total}$ is the total metal concentration as determined following the complete dissolution of the black mass material in concentrated 8.0 mol L^{-1} HCl using a 25 g L^{-1} solid to liquid ratio and temperature of 353 K. Within the standard deviation of triplicate dissolution experiments, all determined black mass chemistries aligned with the theoretical stoichiometry apart from NMC_{111} in which a small excess of manganese was measured to yield a final composition of $LiNi_{0.33}Mn_{0.35}Co_{0.33}O_2$.

Metal recovery

Metal recovery was performed by oxalic acid precipitation after adjusting the pH to 4.0 ± 0.1 with ammonia 25 vol%. However, upon adjusting the pH to 4.0 and before the addition of oxalic acid, a nickel-rich precipitate was formed. After filtration and solid recovery, oxalic acid was subsequently added in a 1.1 molar equivalent to the filtrate yielding a second precipitate. The collected precipitates were individually dried overnight in the oven at (323 ± 1) K. The samples were placed in a combustion furnace at (823 ± 1) K for 8 h to improve their crystallinity and subsequently characterized by powder X-ray diffraction (XRD). A small portion of each precipitate was fully digested with HCl 37 wt% and the metal content was verified by TXRF and Li(I) ion-selective electrode.

Results and discussion

Characterization of the acidified Black Liquor

To ensure the proposed use of BL residue is compatible with existing industrial lignin valorization processes, such as the "LignoBoost" process for lignin isolation from BL,[36] the industrially obtained BL was acidified until pH = 2.0. Additionally, pre-acidification of the BL prior to contacting it with the leaching solution avoids the risk of unwanted precipitation and acid neutralization due to the alkaline nature of the raw BL (pH ~14.0). The composition of BL after adjustment to pH = 2.0 was characterized by GC-MS, with different compound family groups being identified. The relative total intensity of each group and the most representative compound within each family is represented in Figure 1. Only compounds with an 85% matching from the MS database were included in Figure 1 with the rest labelled as "unassigned", a detailed breakdown of the pretreated BL composition is available in Table S1 in the Supporting Information. The aim of the BL characterization is not to provide an exhaustive description of its composition but rather to provide a baseline for comparison after leaching to better understand its reducing mechanism.

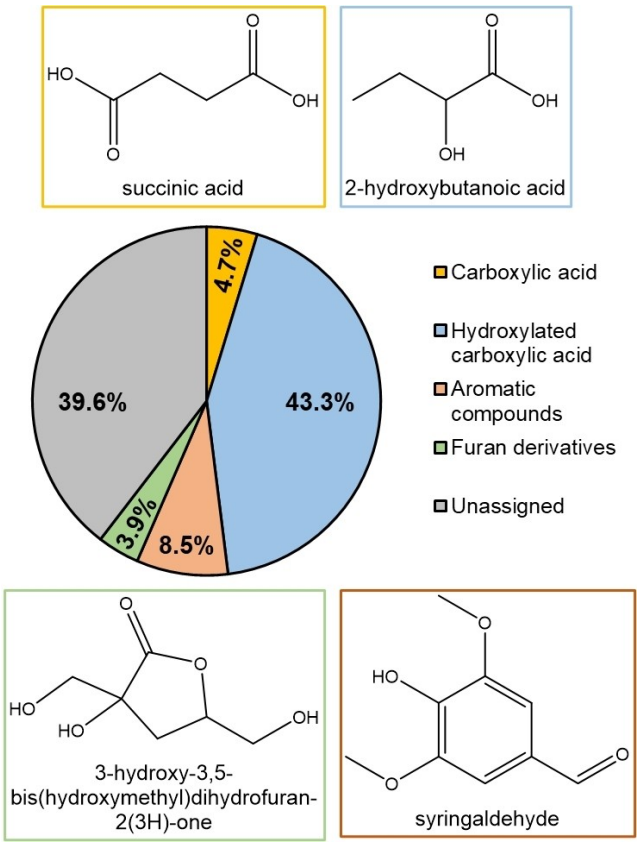

Figure 1. Relative total intensity of each compound family along with structures of the most representative compound for each. Compounds with matching percentage from the MS database below 85% were labelled as "unassigned", see Table S1 for more details.

The hydroxylated carboxylic acid family, which includes the major compounds 2-hydroxybutanoic acid and 3-hydroxypropanoic acid, is the most significant in the acidified BL composition. This is followed by aromatic compounds (syringaldehyde, 2-(3,4-dimethoxyphenyl)-2-hydroxyacetic acid, gallic acid, and syringic acid), carboxylic acids (succinic acid, oxalic acid, and 2-methylsuccinic acid), and furan derivatives. Several functional groups are expected to exert reducing power, including carbonyl, hydroxyl, aldehydes, and ketones.[37] Compounds having aromatic rings are also anticipated to act as reducing agents. Among the identified compounds, the hydroxylated carboxylic acid known as 2-hydroxybutanoic acid emerged as the most abundant, accounting for 38.4% of the relative total intensity (Table S1). This hydroxylated carboxylic acid is usually the most abundant within this class of compounds.[28] It is formed through the isomerization of the xylan-reducing end group into a pentulose, followed by a subsequent beta-elimination reaction. During the pulping process, volatile acids such as acetic and formic acid are produced. Acetic acid is generated by the deacetylation of acetyl groups present in hemicellulose during the initial delignification phase, while formic acid is formed uniformly during the peeling reaction.[38]

Although the BL is expected to contain considerable amounts of acetic and formic acid, their quantification was not possible through this methodology.[28,39] Besides the dissolved wood degradation products, BL also contains sodium and sulfides originating from the inorganic Kraft pulping chemicals NaOH and Na_2S.[27] However, similarly to acetic and formic acid, their quantification *via* GC was not feasible.

Influence of black liquor concentration

The reducing power of acidified BL is expected to boost metal leaching from cathode powder. The leaching efficiency was evaluated using a cathode powder with an NMC_{111} chemistry; the BL vol% was varied from 0 to 50 vol% whilst maintaining a H_2SO_4 concentration of 2.0 mol L^{-1} and an arbitrarily selected initial leaching conditions of 4 h and 333 K to better understand the influence of BL on the dissolution of NMC_{111} (Figure 2A). A systematic optimization of the leaching conditions as well as the influence of the BL composition on the NMC_{111} dissolution is presented further on.

The cathode powder dissolution in a sulfuric acid medium is expected to occur as described in Equation 3:[40]

$$4LiMO_{2,(s)} + 6\ H_2SO_{4,(l)} \leftrightarrow 2Li_2SO_{4,(l)} + 4\ MSO_{4,(l)} + 6H_2O_{(l)} + O_{2,(g)} \quad (3)$$

where M = Co, Mn, or Ni and the subscripts indicate the solid, liquid, or gaseous phase. Theoretically, complete metal dissolution requires a stoichiometric excess of 1.5 H_2SO_4 relative to cathode powder without a reducing agent. The molar excess of H_2SO_4: NMC_{111} is 5.0 for 2.0 mol L^{-1} of H_2SO_4 and as such complete dissolution is expectable under such conditions even considering the partial dissociation of H_2SO_4 and the presence of HSO_4^- species ($pKa_2 \approx 2.0$). However, in the absence of BL only moderate leaching of Ni(II) and Co(II) was observed whilst a negligible Mn(II) concentration was measured in solution. These results are consistent with the identification of chemical reaction as the rate limiting step for the dissolution of LIB cathodic black mass in the absence of a reducing agent and the high activation energies.[41] For reference, the standard reduction potential of the Mn(IV)/Mn(II) and Co(III)/Co(II) pairs in acidic media is of 1.23 V and > 1.90 V respectively *vs* SHE.[42,43] Additionally, previous studies demonstrated that following an initial leaching, the Mn(II) content gradually decreases with time as the redox potential of the H_2SO_4 leachate reaches values close to 1.40 V *vs* SHE and exceeds the reduction potential of the MnO_2/Mn^{2+} redox pair, resulting in the precipitation of the insoluble MnO_2.[41,44] It is also worth noting that in the absence of H_2SO_4, a 50 vol% acidified BL solution (dashed line in Figure 2A) only yielded a final leaching percentage of 9.6 ± 0.5%, 6.5 ± 0.3%, and 8.4 ± 0.4% for Mn(II), Co(II), and Ni(II) respectively.

Raising the acidified BL vol% results in improved leaching efficiencies for all metals, clearly demonstrating the positive synergistic effect of the mixture. A linear relation between the BL vol% and the leaching of Mn(II) is obtained ($R^2 > 0.94$) as shown in Figure 2B, with the best overall leaching efficiencies attained at 50 vol% of BL. The improved leaching yields are assigned to the increased concentration of reductive species, identified in Figure 1, in the leachate with increased BL volume percentage. In contrast, the leaching efficiency of Co(II) and Ni(II) appears independent of the acidified BL vol% until the leaching yield of Mn(II) exceeds that of the other transition metals, after which an increase is observed. This is clearly represented in the case of Co(II) in Figure 2B, suggesting that the primary impact of BL is on the reduction of manganese to its +2 oxidation. The subsequent increase in Co(II) and Ni(II) leaching yield upon improved Mn(II) dissolution ([BL] > 30 vol%) is assigned to (i) removal of the passivating manganese oxide layer shell around the NMC_{111} core and (ii) the ability of Mn(II) to act as an *in-situ* reductant for further NMC_{111} leaching.[41] The leaching yield of Li(I) is significantly better than the remaining metals, especially at lower BL vol% and is not

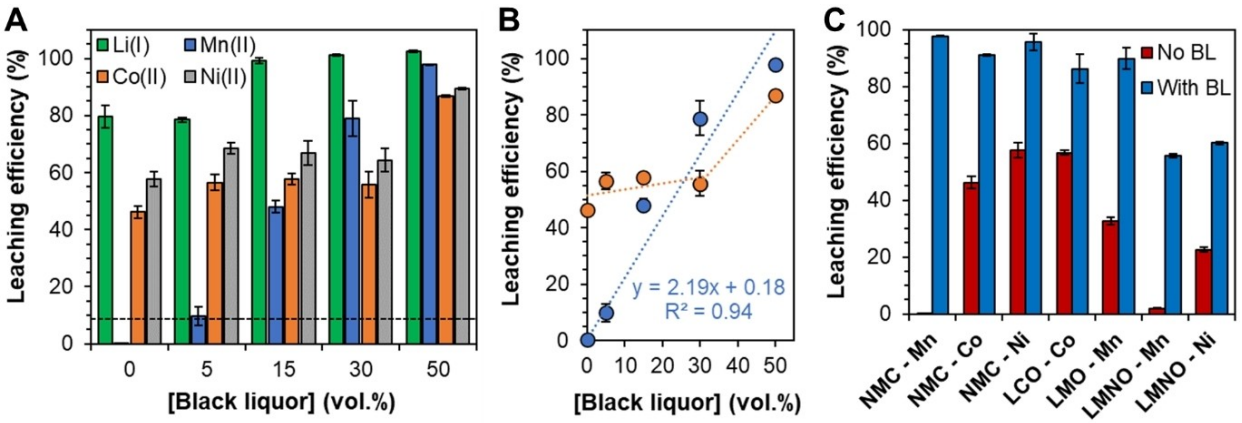

Figure 2. (A) Influence of the acidified BL vol% in the leaching efficiency of NMC_{111} at a fixed H_2SO_4 concentration of 2.0 mol L^{-1}. The dashed line represents the Mn(II) leaching efficiency in 50 vol% acidified BL in the absence of H_2SO_4. (B) Correlation between metal leaching efficiency and the acidified BL vol% (element color code and leaching efficiency values are the same as in panel (A)). (C) Influence of 50 vol% acidified BL in the leaching of several LIBs cathode chemistries in the presence of 2.0 mol L^{-1} H_2SO_4 (LCO – $LiCoO_2$; LMO – $LiMn_2O_4$; LMNO – $LiMn_{1.5}Ni_{0.5}O_4$). Unless otherwise specified, leaching conditions of $T = 333$ K, solid:liquid ratio of 25 g L^{-1}, 300 rpm, and $t = 4$ h were applied.

significantly impacted by its presence. A similar behavior was reported in HCl and H_2SO_4 leaching media.[13,41]

The transferability of the proposed approach to other LIB chemistries and inorganic acid (H_2SO_4 *vs* HCl) was further investigated to better appreciate its applicability. The versatility of acidified BL as reducing agent for LIB lixiviation with various cathode compositions, namely NMC_{111}, LCO, LMO and LMNO, was explored by comparing the leaching efficiency of the transition metals using 2.0 mol L^{-1} H_2SO_4 with and without addition of 50 vol% of BL. As shown in Figure 2C, significant leaching improvements are obtained upon acidified BL addition, with the extent of the improvement being particularly beneficial for Mn-containing active cathode materials. Without BL, the leaching efficiency of Mn(IV) ranged from 0.2 to 32.8%. The digestion of Mn-rich cathodes is typically more challenging due to their enhanced stability.[13,45] The oxidation states of the metals within each cathode are expected to be primarily Li(I), Ni(II), Co(III) and Mn(IV).[46,47] Since Mn(IV) has the highest valency, its leaching is greatly hampered without the introduction of a reducing agent. Similarly, other reports observed low leaching efficiencies for both Mn(IV) and Co(III) in the absence of a reducing agent due to the inability to reduce these high-valency metals into the readily soluble Mn(II) and Co(II) ions.[13,48,49] The proposed leaching approach exhibits good resilience when applied to various cathode chemistries, achieving near-complete leaching in most cathode powders. Although the leaching of LMNO was significantly enhanced in the presence of BL, the leaching efficiencies of Mn(II) and Ni(II) remained below 60%. This is most likely due to the use of a fixed acid concentration that was not adjusted to reflect the varying molecular weight between the different chemistries.

The influence of acid selection was evaluated using a cathode powder with an NMC_{111} chemistry, by assessing the efficiency of 2.0 mol L^{-1} HCl with and without 50 vol% BL, with the results presented in Figure S1 of the ESI. In contrast to H_2SO_4, significantly better leaching yields were obtained when using HCl alone, resulting in a trivial increase upon the addition of BL. Considering that HCl is a stronger acid than H_2SO_4 and that the presence of chloride ions prevents manganese compound precipitation,[44,45] the influence of BL on the leaching process is expected to be more significant when using H_2SO_4. Overall, the leaching efficiency of the H_2SO_4 medium is better than that of the HCl medium at the same acid (2.0 mol L^{-1}) and BL (50 vol%) concentration.

Leaching mechanisms – structural evolution

The dissolution mechanism of LIBs typically occurs *via* a two-step mechanism. The first dissolution step is kinetically rapid (on the time scale of minutes) and controlled by the acid-induced delithiation of the active cathode material whilst the slower second step is governed by the surface reorganization from the layered NMC_{111} structure to a metastable phase arising from the disproportionation reaction of Mn.[41,45] To better appreciate the LIB dissolution mechanism upon addition of acidified BL, the residual NMC_{111} solid fractions after leaching using 2.0 mol L^{-1} H_2SO_4 and various BL volume fraction from 0 to 50 vol% as in Figure 2A were analyzed by powder XRD. The resulting XRD diffractograms are presented in Figure 3, the almost complete dissolution of the NMC_{111} when using 50 vol% acidified BL prevented its analysis.

The deintercalation of lithium induces charge compensation by the transition metals, generating one electron *per* each lithium removed.[41] The charge is compensated by the Ni(II)/Ni(IV) pair up to the deintercalation of 2/3 of Li(I).[50,51] In the range $2/3 \leq x \leq 1$, the charge compensation is undertaken by the Co(III)/Co(IV) pair. Mn(IV) remains electrochemically inactive, stabilizing the structure. The particle surface is then depleted in lithium and the transition metals are oxidized. The vacancies caused by delithiation are occupied by migrating transition metals, lowering electrostatic repulsions, and leading to the shift of the (003), (102), and (104) planes of NMC_{111} (Figure 3, symbol ▲) to higher 2θ values upon leaching with 2.0 mol L^{-1} H_2SO_4 (Figure 3, symbol ●).[41] The NMC_{111} only undergoes partial delithiation when leached with a 2.0 mol L^{-1} H_2SO_4 solution. The transition metal rearrangements form a new spinel-type structure composed of monoclinic structure crystals with Mn_4O_8 coordinated with water molecules (Figure 3, symbol ■), visible at BL vol% ranging from 0 to 15 vol%. The addition

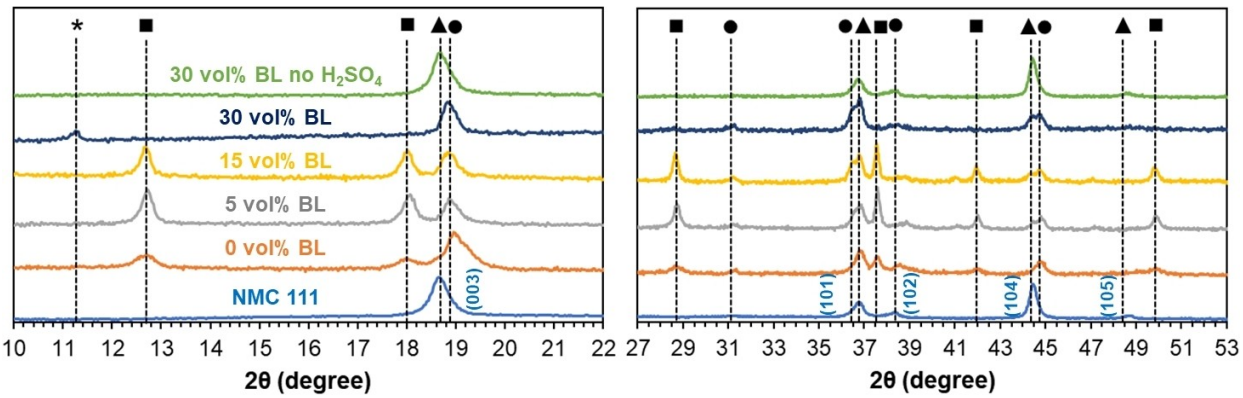

Figure 3. Zoom-in of the powder XRD pattern of the NMC_{111} residue from 10 to 53 degrees and peak assignment for NMC_{111}. The symbols presented in the XRD spectra represent the following: ▲NMC_{111} ($LiCo_{0.33}Ni_{0.33}Mn_{0.33}O_2$; PDF – 04-014-7600), ■ $Mn_4O_8(H_2O)_{0.60}$ (PDF – 04-014-3553) and ● depleted lithium material of the LNMO type $Li_{(1-n)}Mn_xNi_yCo_2O_2$ where $0 < n < (x+y+z)$. Leaching conditions are identical to those in Figure 2A.

of BL leads to an increased formation of Mn(IV) oxides with a subsequent change in their corresponding relative peak intensities. The leaching of Ni(II) and Co(II) seems to be governed by Mn(II/IV) formation. As the acidified BL vol% increases up to 30 vol%, the extraction of Co(II) and Ni(II) remains dormant while the concentration of Mn(II) exhibits an upward trend (Figure 2B). At 30 vol% of BL, the concentration of Mn(II) in the leachate is similar to those of Co(II) and Ni(II) and the Mn(IV) oxide peak disappears. From this point onward, the Co(II) and Ni(II) leaching is unlocked, leading to near-complete extraction. Whilst leaching with 2.0 mol L^{-1} H_2SO_4 causes partial delithiation and the formation of Mn(IV) oxides, the addition of only BL does not influence the crystalline structure of NMC_{111}, demonstrating a synergistic influence of H_2SO_4 and BL concentration.

Leaching mechanisms – liquid phase evolution

Attention is now paid to the change of the acidified BL composition under varying leaching scenarios. The aromatic content of the BL was monitored by HPLC before and after the NMC_{111} leaching process whilst GC-MS analysis of the solution after leaching was also carried out and compared to that reported in Figure 1 and Table S1. The composition of BL, BL + NMC_{111} and BL + NMC_{111} + H_2SO_4 was further evaluated by FTIR. All samples were maintained at $T = 333$ K for 4 h with a mixing speed of 300 rpm prior to analysis. In the sample containing NMC, a solid to liquid ratio of 25 g L^{-1} was applied whilst the H_2SO_4 concentration was maintained at 2.0 mol L^{-1}. The involvement of the BL in metal leaching is demonstrated by HPLC analysis (Figure 4A). Importantly, no differences in the chromatograms of the acidified BL with that of the 50 vol% BL with H_2SO_4 were observed (Figure S2 of the ESI), suggesting that any changes in the chromatograms between samples is not directly due to the degradation of the aromatic content by the acid.

Although minimal transition metal leaching was observed upon contacting NMC_{111} with acidified BL in the absence of added H_2SO_4, the resulting chromatogram after contact shows significant alterations when compared to the BL chromatogram. Notably, most of the aromatic peaks present in the original acidified BL are diminished or disappear, with one prominent peak appearing at a retention time of 16.8 min. The latter indicates the formation of intermediate products during the reduction reaction. Unfortunately, the compound with a retention time of 16.8 min could not be identified despite the injection of various standards. Although outside the scope of this current work, the results in Figure 4A hint at the possibility of using waste LIB cathode material as catalyst for the simplification of the BL aromatic content and the production of higher value compounds. Addition of 2.0 mol L^{-1} H_2SO_4 to the mixture of 50 vol% acidified BL and NMC_{111} yields a chromatogram with no discernable aromatic peaks, as shown in red in Figure 4A. According to the Folin-Ciocalteu method,[33] a 50 vol% acidified BL contains a total phenolic content of (1.7 ± 0.1) g L^{-1} expressed as gallic acid equivalents. Phenolic compounds contain at least one hydroxyl group that can act as a reducing agent, prompting the leaching of higher valence oxides. The

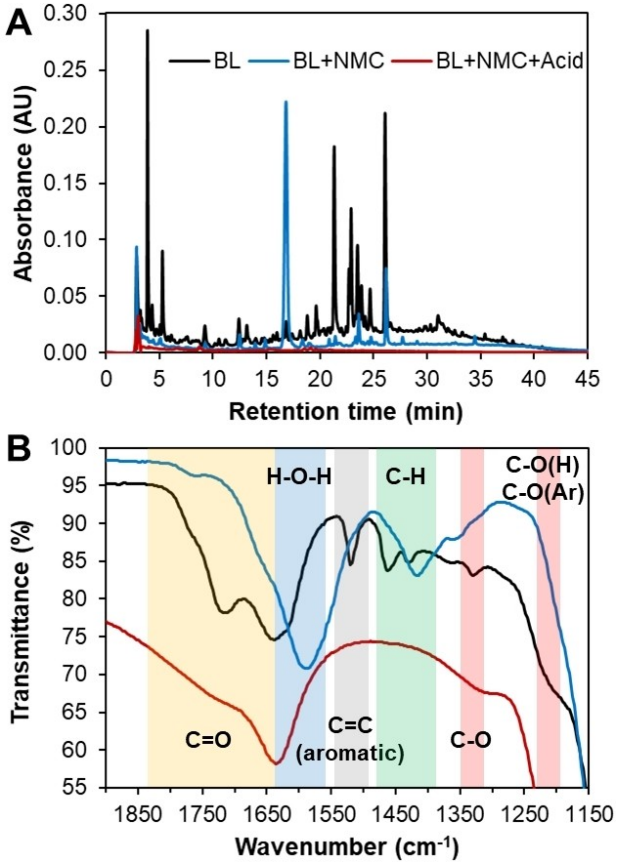

Figure 4. (A) HPLC chromatogram and (B) FTIR spectra of the acidified BL (black line), acidified BL after contact with 25 g L^{-1} NMC_{111} (blue), and acidified BL after contact with 25 g L^{-1} NMC_{111} and 2.0 mol L H_2SO_4 (red). All samples were maintained at 333 K for 4 h prior to analysis.

involvement of these aromatic compounds in metal leaching is well depicted by the disappearance of their corresponding peaks in the HPLC spectrum after NMC_{111} leaching. Although the used HPLC equipped with a UV detector is designed to detect aromatic compounds, it is expected that other elements present in the BL, namely mono- and di-carboxylic acids through the formation of aqueous metal complexes, contribute positively to the dissolution of transition metals.

Due to the intricate composition of BL (Table S1) it is challenging to identify the key components for the redox dissolution of metals. The FTIR spectra exposes some of the functional groups involved in NMC_{111} leaching (Figure 4B, full spectra available in Figure S3). The close involvement of ketone and carbonyl groups in the leaching of NMC_{111} is depicted by the decrease of the C=O band at 1714 cm^{-1},[52] although the partial overlap of the water band at 1640 cm^{-1} complicates the analysis. The C=C aromatic band at 1519 cm^{-1} disappears upon contact with NMC_{111}, regardless of the presence of H_2SO_4. This alteration suggests that the alkenes/aromatic compounds undergo oxidation during the leaching reaction, degrading the original compound.[53] The peak at 1328 cm^{-1} corresponding to the C–O stretching is also altered upon NMC_{111} leaching. Due to their susceptibility to oxidation, the C–O bonds are anticipated to undergo oxidation or transform into different functional

groups during the leaching process. A similar effect is observed at 1209 cm^{-1}, with the disappearance of C–O bands in aliphatic and aromatic compounds. The changes in the HPLC and FTIR spectra after NMC_{111} leaching are corroborated by the GC-MS analysis of the final leaching solution, summarized in Table S2. An almost complete disappearance of aromatic compounds was observed and an increased formation of oxidation products, primarily simple mono-hydroxylated and dicarboxylic acids including lactic acid, 2-hydroxybutyric acid, glycolic acid, butanoic acid, pentonic acid, glutaric acid, hydracrylic acid, and oxalic acid. Overall, the data from HPLC, GC-MS and FTIR indicate the active engagement of oxygenated and aromatic groups, suggesting that these chemical groups are essential for an efficient leaching reaction and that the resulting BL oxidation products can further promote the transition metals dissolution. Based on the analytical results, the possible leaching reaction can be expressed as Equation 4:

$$\alpha LiMO_{2,(s)} + \beta H_2SO_{4,(l)} + \gamma BL_I \leftrightarrow \frac{\alpha}{2}Li_2SO_{4,(l)} + \alpha MSO_{4,(l)} + \beta H_2O_{(l)} + \delta OP \quad (4)$$

where OP represents the BL oxidized products.

The complexity of BL conceals the influence of its components as individual reducing agents. To better understand which components are vital for the redox potential of BL, several representative compounds were paired with 2.0 mol L^{-1} H_2SO_4 at a 0.1 mol L^{-1} concentration to evaluate their influence on the leaching efficiency of NMC_{111}. The reducing agents were carefully selected. Gallic acid was chosen to represent aromatic carboxylic acids, while vanillin was selected to embody the aromatic alcohol group. Considering that the reducing agent concentration (0.1 mol L^{-1}) is above the aqueous solubility limit of gallic acid and vanillin, these compounds were added as a suspension. Ethanol and glucose, frequently recognized as alternative green reducing agents, were selected as representatives of the alcohol and sugar family.[18,54,55] Since BL is also expected to contain inorganic compounds, the role of $Na_2S_2O_3$ and $FeSO_4$ as reducing agents was evaluated. Lastly, due to the substantial content of carboxylic acids in BL, acetic acid was included in this assay as a representative compound. The leachate from one of the most promising reducing agents was analyzed by HPLC before and after NMC_{111} leaching and the obtained precipitate was analyzed by XRD. The experimental results are represented in Figure 5. When reported, the relevant first redox couples for the tested compounds in Figure 5 are listed in Figure S3 of the supporting information.

The leaching efficiency of the evaluated reducing agents increases as follows: acetic acid < $Na_2S_2O_3$ < $FeSO_4$ < ethanol < glucose ≈ vanillin ≈ gallic acid. Apart from acetic acid, adding a reducing agent improves the overall leaching efficiency. The performance of the reducing agents is intertwined with their redox potential. Acetic acid is a weak acid with only one hydrogen bond donor arising from its carboxylic group. Carboxylic acids have a relatively high oxidation state, leading to a subpar reducing power and low leaching efficiencies. Similarly to acetic acid, the inorganic compounds $Na_2S_2O_3$ and $FeSO_4$ yield mediocre leaching efficiencies. According to Zhang *et al.*,[56] $Na_2S_2O_3$ can be an efficient reducing agent for NMC_{111} leaching but only at concentrations above 0.2 mol L^{-1}. Although $FeSO_4$ has a similar redox potential to conventional reducing agents (Fe^{3+}/Fe^{2+} $E^0 = 0.77$ V), it still afforded poor leaching results. These inorganic compounds may require harsher leaching conditions to achieve complete leaching.[57]

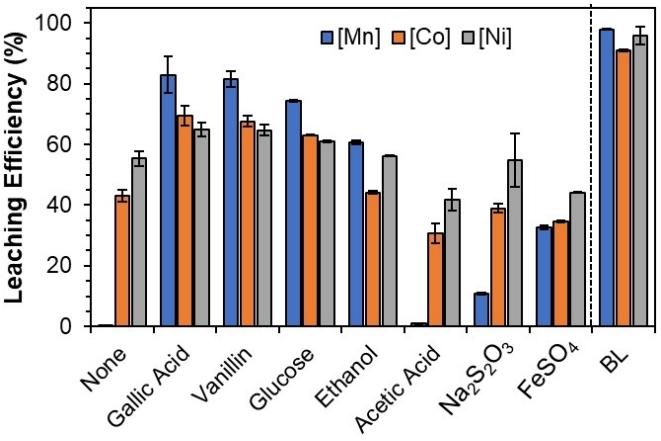

Figure 5. Effect of different reducing agents in the leaching efficiency of NMC_{111} using 2.0 mol L^{-1} of H_2SO_4 at (333 ± 1) K, solid:liquid ratio of 25 g L^{-1}, 300 rpm and 4 h.

The best leaching results were observed for compounds containing hydroxyl groups. Ethanol afforded poorer results than gallic acid, glucose, and vanillin since it only possesses one hydroxyl group and no other oxidizable functional group. The successful application of ethanol as a reducing agent has been previously reported but it may require harsher leaching conditions.[18] Unlike ethanol, the addition of gallic acid, vanillin and glucose exhibits an interesting amount of oxidizable functional groups, including hydroxyl and/or aldehyde groups. These functional groups can exert reducing power and partake in redox reactions involving high-valency metals. For instance, the redox potential of phenol (E^0 *vs* SHE) is enhanced from 0.99 to 0.61, 0.97 and 0.53 when substituted with another hydroxyl group in the *ortho*-, *meta*- or *para*- position, respectively.[58]

Gallic acid is a polyhydric compound having two hydroxyl groups in the *meta*- position and one in the *para*- position, whereas vanillin displays one hydroxyl group in the *para*- position. The aldehyde group of vanillin can undergo oxidation to form vanillic acid, granting it a good reducing potential.[59] The HPLC chromatogram depicts the structural modification of vanillin following NMC_{111} leaching (Figure S4). After NMC_{111} leaching, the intensity of the HPLC peak corresponding to vanillin is noticeably diminished, suggesting its oxidation and cleavage of the aromatic moieties. Interestingly, a white precipitate was formed during the leaching reaction. Its composition was determined using XRD analysis, revealing the presence of divanillin alongside $CoSO_4 \cdot 6H_2O$ stemming from the incomplete washing of the leachate from the precipitate (Figure S5). Such intermediate compounds as divanillin arising from the degradation of the BL in contact with NMC_{111} are powerful reducing agent, with an estimated reducing potential ranging from −2.00 to −1.75 V (E^0 *vs*

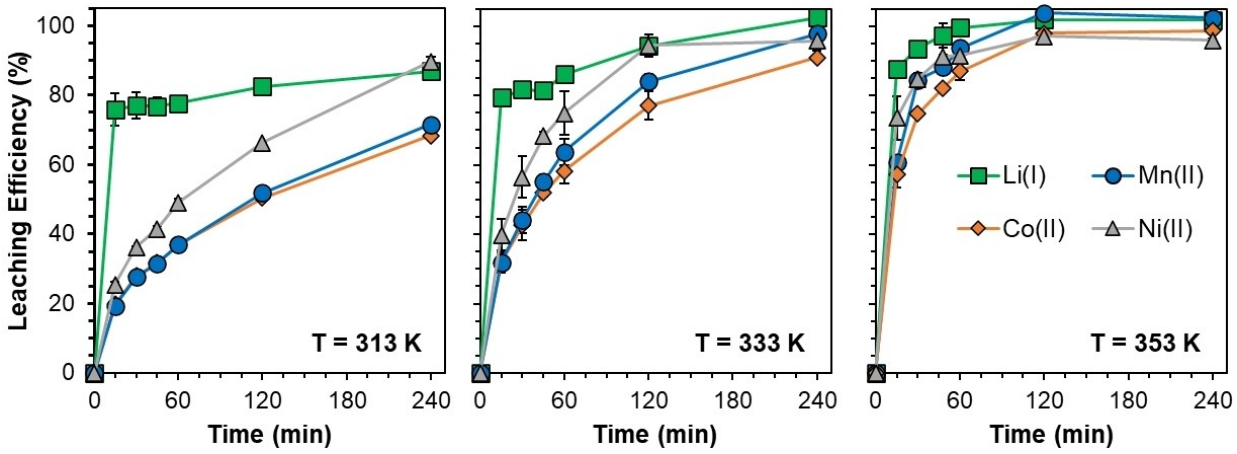

Figure 6. Temperature effect at 313 K, 333 K and 353 K (±1 K) on the metals leaching efficiency in a 2.0 mol L^{-1} H_2SO_4 solution with 50 vol% BL at a solid: liquid ratio of 25 g L^{-1}, and 300 rpm.

SHE) further promoting the dissolution of manganese.[60] Since divanillin is less water-soluble than vanillin (0.29 *vs* 6.9 mg L^{-1}, respectively), it precipitates upon its formation.[61] To summarize, the performance of BL surpasses that of all the other evaluated compounds, indicating that the reducing potential of BL is likely attributed to the combined effect of multiple compounds within its composition.

Kinetic analysis and comparison with other renewable reductants

To gain further insight into the metal dissolution mechanisms using 50 vol% of acidified BL and 2.0 mol L^{-1} H_2SO_4 as a leaching medium, the effect of temperature on metal leaching kinetics was evaluated. The dissolution kinetics at 313 K, 333 K, and 353 K are presented in Figure 6.

The leaching extraction efficiency improves as temperature increases from 313 to 353 K. Optimal leaching is obtained at 353 K after 2 h leaching with (102.0 ± 0.8)% Li(I), (98.0 ± 1.6)% Co(II), (103.8 ± 2.7)% Mn(II) and (97.1 ± 0.7)% Ni(II) extracted. Similar results were obtained at 333 K after 4 h leaching with (102.5 ± 0.3)% Li(I), (91.0 ± 0.4)% Co(II), (97.8 ± 0.2)% Mn(II) and (95.8 ± 2.9)% Ni(II) extracted. Leaching efficiencies greater than 100% are most likely due to small experimental errors occurring during sample preparation and quantification. During the kinetic assay at 353 K, the composition of the leachate was monitored using HPLC to identify the aromatic compounds involved in NMC_{111} dissolution. An almost complete degradation of the aromatic components of the acidified BL was observed after just 15 min as shown in Figure S6. Interestingly, new peaks in the HPLC chromatogram appeared after 15 min before disappearing with time up to 120 min, representing the time required for the almost quantitative dissolution of NMC_{111}. Two peaks of the HPLC spectra corresponding to intermediate compounds not originally present in the acidified BL were visibly altered across time and the correlation between their absorbance and leaching time is shown in Figure 7. The

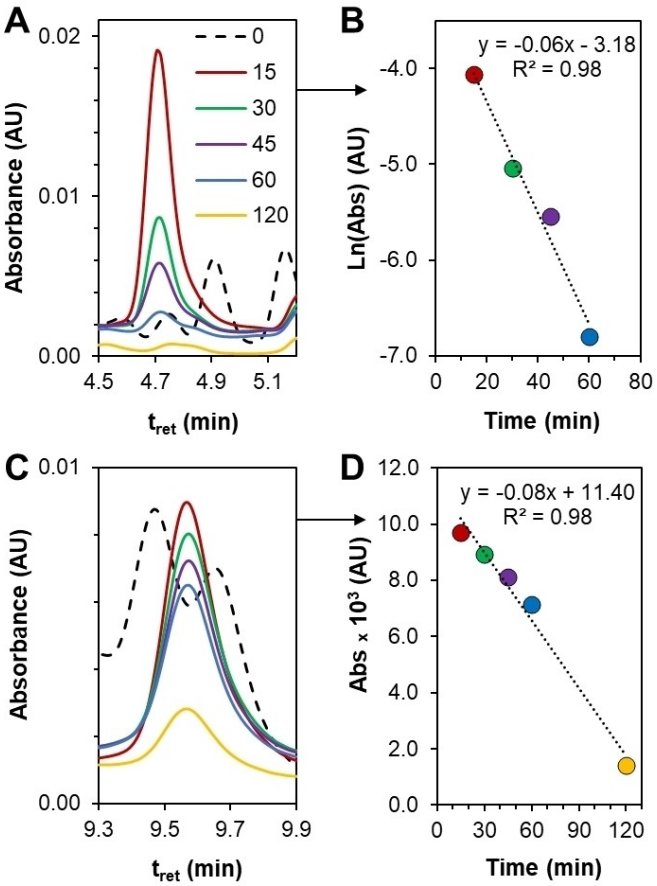

Figure 7. (A,C) HPLC chromatograms of the acidified BL after NMC leaching at 353 K as a function of the leaching time and (B, D) the corresponding kinetic fitting of the intermediate oxidation products degradation.

intensity of the peaks observed at retention times of 4.7 and 9.6 min decreases as the leaching reaction occurs, however the apparent rate constant for the degradation reaction of the intermediate products are first and zero order respectively (ln(Abs) *vs* t and Abs *vs* t). The results in Figure 7 suggest the occurrence of multiple parallel redox reactions, each with its

Table 1. Kinetic parameters for Li(I), Co(II), Ni(II), and Mn(II) at 313 K, 333 K, and 353 K (±1 K) given by all the adjusted empirical models.

		Li(II)		Co(II)		Mn(II)		Ni(II)	
	T (K)	k (min^{-1})	R^2	k (min^{-1})	R^2	k (min^{-1})	R^2	k (min^{-1})	R^2
SCM reaction	333	0.17	0.64	0.09	0.93	0.10	0.94	0.14	0.96
	353	0.34	0.92	0.20	0.96	0.28	0.97	0.22	0.95
	373	0.95	0.94	0.57	0.96	0.99	0.96	0.85	0.96
SCM diffusion	T (K)	k (min^{-1})	R^2	k (min^{-1})	R^2	k (min^{-1})	R^2	k (min^{-1})	R^2
	333	0.17	0.70	0.06	1.00	0.07	1.00	0.13	0.99
	353	0.20	0.88	0.17	1.00	0.20	1.00	0.33	1.00
	373	1.05	0.96	0.53	0.99	0.70	0.99	0.84	0.98
SCM mixed-controlled	T (K)	k (min^{-1})	R^2	k (min^{-1})	R^2	k (min^{-1})	R^2	k (min^{-1})	R^2
	333	0.09	0.83	0.02	0.97	0.02	0.96	0.08	0.89
	353	0.32	0.98	0.06	0.96	0.26	0.87	0.22	0.94
	373	1.40	0.99	0.28	0.99	0.52	0.97	0.50	0.98

own reaction rate contributing to the overall reduction leaching of NMC_{111}. Several standard compounds were analyzed by HPLC in an attempt to assign the peaks at 4.7 and 9.6 min. Despite the efforts, it was not possible to unequivocally identify these compounds. Nevertheless, it is evident that the leaching process occurs via a multiple step mechanism with the alteration of and subsequent degradation of intermediate aromatic compounds in the presence of NMC_{111}.

The experimental data in Figure 6 were fitted with three models based on shrinking core models (SCM) assuming spherical particles to better understand the underlying leaching mechanisms, as shown in Equations 5–7:

$$1-(1-x)^{\frac{1}{3}}=kt \tag{5}$$

$$1-3(1-x)^{\frac{2}{3}}+2(1-x)=kt \tag{6}$$

$$\left[(1-x)^{-\frac{1}{3}}-1\right]+\left(\frac{1}{3}\right)\ln(1-x)=kt \tag{7}$$

where x is the fraction reacted in time t (min) and k (min^{-1}) is the overall specific rate constant of each model. Equation 5 represents the surface chemical control model, while Equation 6 corresponds to the diffusion control model and Equation 7 describes a mixed-controlled that combines film diffusion and chemical reaction. All fittings are represented in Figure S7 of the ESI and are summarized in Table 1.

The diffusion control model yielded the best correlation plots for Li(I), Co(II), Ni(II) and Mn(II) among the tested fittings. The Li(I) fit was poor regardless of the tested model, subsequent derived values from Li(I) rate constants must be carefully considered. The reaction rate constants extrapolated from the diffusion control model (Equation 6) at different temperatures was used to determine the apparent activation energies (E_a) of Co(II), Mn(II) and Ni(II). The E_a values were calculated according to the Arrhenius equation (Equation 8) and the resulting plots are depicted in Figure 8.

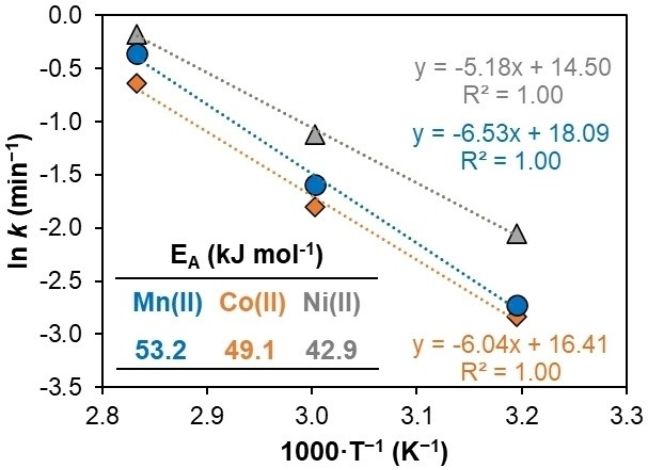

Figure 8. Arrhenius plot for the leaching of Co(II), Mn(II) and Ni(II) in 2.0 mol L^{-1} H_2SO_4 with 50 vol% BL.

$$\ln k=\ln A-\frac{E_a}{RT} \tag{8}$$

where A is the frequency factor, E_a is the apparent activation energy (J mol^{-1}), R is the gas constant (8.314 J mol^{-1} K^{-1}) and T is the temperature (K). The activation energy for the leaching of each metal can be extrapolated from the slope of each ln$k$ vs 1000 T^{-1} plot. The activation energies of Li(I) (not show, regression R^2 = 0.93), Co(II), Mn(II) and Ni(II) are 30.0, 49.1, 53.2 and 42.9 kJ mol^{-1} respectively. Despite the diffusion control model being a better fit for the data, the obtained activation energies exceed 40 kJ mol^{-1}, which falls within the range of chemical reaction-controlled leaching.[62,63] As a consequence, the occurrence of a mixed diffusion-reaction process cannot be dismissed.

Overall, the obtained activation energies are within the reported range (≈35 to 60 kJ mol^{-1} for transition metals) for the reductive LIB leaching in H_2SO_4 with conventional H_2O_2[64] and various biomass derived reductants including ethanol,[18] tea waste,[24] bacterial waste,[65] and plant waste.[66] The leaching conditions across these various leaching systems are summar-

ized in Table 2, showing that the application of BL compares well against most other reducing agent in terms of process variables. Herein, the quasi-quantitative dissolution of all NMC_{111} component was achieved using moderate H_2SO_4 concentrations, comparable or smaller leaching times and temperatures, and a greater solid-to-liquid ratio relative to other reductive leaching studies of BM in H_2SO_4. Further work is required to make the application of BL competitive with the industrially established H_2O_2 reducing agent, the latter was shown to operate at an improved solid-to-liquid ratio (100 *vs* 40 g L^{-1}) and half the leaching time (60 *vs* 120 min).[64] This work proposes a novel route to the valorization of BL compatible with the recovery of lignin. By relying on the reductive characteristics of the various components in the BL rather than a single high purity reducing agent, production and associated environmental costs of the reducing agent can be mitigated.

Metal recovery

Metal recovery is a critical and indispensable step in cathode recycling, as it enables closing the loop by effectively reclaiming valuable metals for reuse. Chemical precipitation is a viable approach to achieve metal recovery and facilitated in this case by the complete degradation of the higher molecular weight organic content of the BL as verified by HPLC. Following the leaching of NMC_{111} under optimized conditions (50 vol% BL, 2.0 mol L-1 H_2SO_4, 353 K, 2 h), for which quantitative leaching of Li(I) and Mn(II) were obtained along with 98.0 Co(II) and 97.1 % Ni(II), oxalic acid was used to precipitate all metals at pH = 4.0 ± 0.1. Ammonia was used as base rather than NaOH as addition of the latter to the leachate resulted in the formation of a white precipitate identified by XRD as Na_2SO_4 hydrate (not shown). However, upon adjusting the pH to 4.0 using ammonia, (17 ± 1)% Co(II), (10 ± 1)% Mn(II) and (41 ± 2)% Ni(II) precipitated without addition of oxalic acid, yielding a final precipitate mass composition of 59.7% Ni(II), 24.8% Co(II) and 15.5% Mn(II) with no Li(I) detected (other elements were not considered). The obtained residue was recovered, calcinated at 823 K and analyzed by XRD (Figure 9A), showing the presence of $Na_2Co(SO_4)_2$ and $NiSO_4$ sulfate salts. This is due to the high ionic strength of the leachate originating both from the initial acidified BL salt content and the subsequent post-leaching pH control, favoring sulfate salt precipitation. Afterwards, oxalic acid was added in a 1.1 molar equivalent excess and (99 ± 2)% Co(II), (75 ± 1)% Mn(II) and (99 ± 1)% Ni(II) of the remaining metals in solution were precipitated for a final mass composition of 38.8% Co(II), 33.6% Mn(II), 27.6% Ni(II) with no Li(I) detected. The obtained residue was also calcinated at 823 K and analysed by XRD (Figure 9B) and shows a mixed cobalt manganese oxide as the primary crystallographic phase of the oxalic acid precipitate after calcination. The absence of nickel in the latter precipitate is likely caused by the similar lattice parameter between Co and Ni manganese oxides and the poor crystallinity of the precipitate. Overall, quantitative recovery of Co(II) and Ni(II) was achieved over two precipitation stages whilst 78% of the total Mn(II) was recovered, confirming the potential of acidified BL as a reducing agent for LIB recycling. Further work is required to extend the recovery process to Li(I) and Na_2SO_4, theoretically achievable by precipitation through the addition of Na_2CO_3 and ethanol respectively,[70,71] and close the resource loop.

Table 2. Reductive cathode leaching conditions and respective metal extraction efficiencies and activation energies reported in the literature using sulfuric acid.

Leaching reactants	T (K)	Time (min)	S/L ratio (g L^{-1})	*EE*%	E_a (kJ mol^{-1})	Ref.
2 mol L^{-1} H_2SO_4	333	240	40	80% Li(II), 46% Co(II), 1% Mn(II), 58% Ni(II)	Not reported	This work
2 mol L^{-1} H_2SO_4 + 5 vol% H_2O_2	348	60	100	99% Li(II), 70% Co(II)	32.4 Li(I), 59.8 Co(II)	64
2.5 mol L^{-1} H_2SO_4 + 20 g L^{-1} oxalic acid	358	100	100	99% Li(II), 97% Co(II), 97% Mn(II), 98% Ni(II)	32.0 Li(I), 47.6 Co(II), 43.0 Mn-(II), 41.0 Ni(II)	67
3 mol L^{-1} H_2SO_4 + 5 vol% ethanol	363	160	20	99% Li(II), 99% Co(II)	37.0 Li(I), 37.6 Co(II)	18
3.0 mol L^{-1} H_2SO_4 + 0.4 g g^{-1} sucrose	368	120	25	100% Li(I), 96% Co(II)	Not reported	68
3.0 mol L^{-1} H_2SO_4 + 0.4 g g^{-1} cellulose	368	120	25	100% Li(I), 54% Co(II)	Not reported	68
1 mol L^{-1} H_2SO_4 + 0.075 M $NaHSO_3$	368	240	20	97% Li(II), 92% Co(II), 88% Mn(II), 96% Ni(II)	20.4 Li(I), 26.8 Co(II), 21.7 Ni-(II)	69
1.25 mol L^{-1} H_2SO_4 + 50 g L^{-1} tea waste	333	60	50	97% Li(II), 84% Co(II), 96% Mn(II), 97% Ni(II)	27.2 Li(I), 27.3 Co(II), 29.0 Mn-(II), 28.5 Ni(II)	24
3 mol L^{-1} H_2SO_4 + 0.8 g g^{-1} antibiotic bacteria waste	363	180	33	100% Li(II), 99% Co(II), 99% Mn-(II), 100% Ni(II)	55.6 Li(I), 53.0 Co(II), 54.7 Mn-(II), 67.2 Ni(II)	65
3 mol L^{-1} H_2SO_4 + 1 g g^{-1} plant waste	363	120	20	99% Li(II), 99% Co(II), 99% Mn(II), 99% Ni(II)	43.5 Li(I), 68.9 Co(II), 81.2 Mn-(II), 80.6 Ni(II)	66
2 mol L^{-1} H_2SO_4 + 50 vol% BL	353	120	40	102% Li(II), 98% Co(II), 103% Mn(II), 97% Ni(II)	49.1 Co(II), 52.3 Mn(II), 42.9 Ni(II)	This work

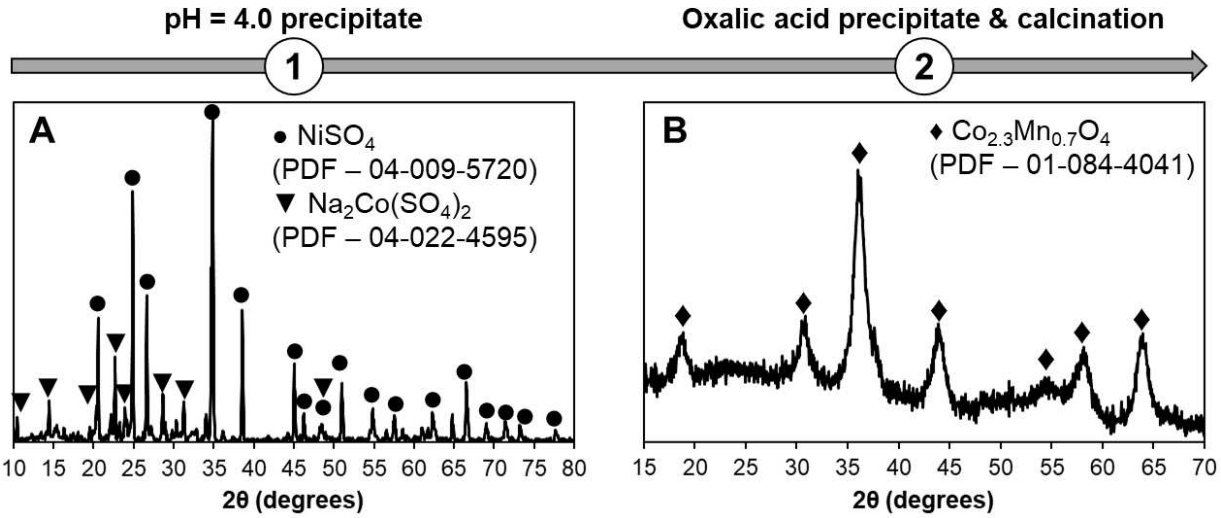

Figure 9. XRD spectra of (A) the precipitate collected after pH = 4.0 adjustment and (B) the precipitate obtained after oxalic acid addition and calcination at 823 K.

Conclusions

In this work, the reductive power of industrial black liquor originating from the Kraft process is applied to the improved leaching of transition metals from LIBs. Importantly, the proposed approach is compatible with the increasing demand for lignin-based products as it uses the residual liquor following lignin precipitation by pH diminution. The proposed H_2SO_4-acidified BL system achieved competitive leaching efficiencies without using unstable reducing agents across a range of LIB cathode chemistries. A linear relation between the BL vol% and the leaching yield of Mn(II) from NMC_{111} was obtained, with the best overall leaching efficiencies being achieved for 2.0 mol L^{-1} H_2SO_4 and 50 vol% of BL at 353 K, suggesting that the primary impact of BL is on the reduction of manganese to its +2 oxidation state and its aqueous stabilization. The latter observation was further validated by the structural study of the solid residue post-leaching clearly showing the emergence and subsequent disappearance of higher valence manganese oxide compounds with an increase in the BL vol%. Characterization of the liquid phase by HPLC, GC-MS and FTIR before and after leaching indicates the degradation of oxygenated and aromatic groups from the BL during NMC_{111} dissolution, suggesting that these chemical groups are essential to promote a reductive environment during reaction and that the resulting BL oxidation products, namely short carboxylic acids, can further promote the transition metals dissolution. Unfortunately, we did not have the required experimental set-up to follow the redox potential of the BL leachate over time, we aim to address this in the future to provide a better understand of the leaching mechanism. Thermodynamic analysis of the leaching process indicates that the presence of BL decreases the leaching activation energy on par with conventional reducing agents such as H_2O_2 and ethanol. Finally, taking advantage of the total degradation of the more complex organic matter during dissolution, the leached transition metals could be easily recovered by pH adjustment and oxalic acid addition. Through the use of a renewable reducing agent, the economic and environmental benefit of H_2SO_4 for the leaching of LIBs are potentiated providing a new avenue for the development of a recycling process with improved sustainability.

Acknowledgements

This work was developed within the scope of the project CICECO-Aveiro Institute of Materials, UIDB/50011/2020, UIDP/50011/2020 & LA/P/0006/2020, financed by national funds through the FCT/MEC (PIDDAC). This work was further supported by national funds through FCT/MCTES (PIDDAC): LSRE-LCM, UIDB/50020/2020 (DOI: 10.54499/UIDB/50020/2020) and UIDP/50020/2020 (DOI: 10.54499/UIDP/50020/2020); and ALiCE, LA/P/0045/2020 (DOI: 10.54499/LA/P/0045/2020). Ana R.F. Carreira acknowledges FCT for the Ph.D. grant SFRH/BD/143612/2019. Nicolas Schaeffer acknowledges the national funds (OE), through FCT-Fundação para a Ciência e a Tecnologia, in the scope of the framework contract foreseen in the numbers 4, 5, and 6 of the article 23, of the Decree-Law 57/2016, of August 29th, changed by Law57/2017, of July 19th. André M. da Costa Lopes acknowledges his research contract funded by the Fundação para a Ciência e Tecnologia (FCT) and project CENTRO-04-3559-FSE-000095-Centro Portugal Regional Operational Programme (Centro2020), under the PORTUGAL 2020 Partnership Agreement, through the European Regional Development Fund (ERDF).

Conflict of Interests

The authors declare no conflicts of interest.

Data Availability Statement

The data that support the findings of this study are available from the corresponding author upon reasonable request.

Keywords: hydrometallurgy · reducing agent · circular economy · leaching · lithium-ion battery

[1] J. J. Roy, S. Rarotra, V. Krikstolaityte, K. W. Zhuoran, Y. D-I. Cindy, Q. Yan, M. Srinivasan, X. Y. Tan, M. Carboni, D. Meyer, Q. Yan, M. Srinivasan, *Adv. Mater.* **2022**, *34*, 2103346.
[2] E. Pomerantseva, F. Bonaccorso, X. Feng, Y. Cui, Y. Gogotsi, *Science* **2019**, *366*.
[3] J. B. Goodenough, K. S. Park, *J. Am. Chem. Soc.* **2013**, *135*, 1167–1176.
[4] P. Xu, D. H. S. Tan, Z. Chen, *Trends Chem.* **2021**, *3*, 620–630.
[5] J. Neumann, M. Petranikova, M. Meeus, J. D. Gamarra, R. Younesi, M. Winter, S. Nowak, *Adv. Energy Mater.* **2022**, *12*, 2102917.
[6] M. Jacoby, *C&EN Global Enterprise* **2019**, *97*, 29–32.
[7] D. J. Garole, R. Hossain, V. J. Garole, V. Sahajwalla, J. Nerkar, D. P. Dubal, *ChemSusChem* **2020**, *13*, 3079–3100.
[8] N. Zhang, Z. Xu, W. Deng, X. Wang, *EER* **2022**, *5*, 1–38.
[9] Critical raw materials, https://single-market-economy.ec.europa.eu/sectors/raw-materials/areas-specific-interest/critical-raw-materials_en, (accessed 15 June 2023).
[10] EU agrees new law on more sustainable and circular batteries, https://ec.europa.eu/commission/presscorner/detail/en/ip 22 7588, (accessed 15 June 2023).
[11] Y. Tao, C. D. Rahn, L. A. Archer, F. You, *Sci. Adv.* **2021**, *7*, 7633.
[12] M. Iturrondobeitia, C. Vallejo, M. Berroci, O. Akizu-Gardoki, R. Minguez, E. Lizundia, *ACS Sustainable Chem. Eng.* **2022**, *10*, 9798–9810.
[13] N. Vieceli, P. Benjamasutin, R. Promphan, P. Hellström, M. Paulsson, M. Petranikova, *ACS Sustainable Chem. Eng.* **2023**, *11*, 9662–9673.
[14] Q. Meng, Y. Zhang, P. Dong, F. Liang, *J. Ind. Eng. Chem.* **2018**, *61*, 133–141.
[15] M. Rana, M. I. H. Khan, T. Nshizirungu, Y. T. Jo, J. H. Park, *J. Chem. Eng.* **2023**, *455*, 140626.
[16] L. Cai, J. Lin, E. Fan, F. Wu, R. Chen, L. Li, *ACS Sustainable Chem. Eng.* **2022**, *10*, 10649–10657.
[17] L. Yao, Y. Xi, H. Han, W. Li, C. Wang, Y. Feng, *J. Alloys Compd.* **2021**, *868*, 159222.
[18] J. Zhao, B. Zhang, H. Xie, J. Qu, X. Qu, P. Xing, H. Yin, *Environ. Res.* **2020**, *181*, 108803.
[19] X. Chen, C. Luo, J. Zhang, J. Kong, T. Zhou, *ACS Sustainable Chem. Eng.* **2015**, *3*, 3104–3113.
[20] Y. Zhang, Q. Meng, P. Dong, J. Duan, Y. Lin, *J. Ind. Eng. Chem.* **2018**, *66*, 86–93.
[21] Z. Wu, T. Soh, J. J. Chan, S. Meng, D. Meyer, M. Srinivasan, C. Y. Tay, *Environ. Sci. Technol.* **2020**, *54*, 9681–9692.
[22] S. Yan, C. Sun, T. Zhou, R. Gao, H. Xie, *Sep. Purif. Technol.* **2021**, *257*, 117930.
[23] L. M. Kustov, A. L. Kustov, T. Salmi, *Mendeleev Commun.* **2022**, *32*, 1–8.
[24] K. Gu, W. Xia, J. Zhou, W. Qin, J. Han, *ACS Sustainable Chem. Eng.* **2023**, *11*, 13606–13615.
[25] M. P. Do, H. K. Lim, C. K. Tan, E. J. J. Tang, M. Srinivasan, C. Y. Tay, *J. Cleaner Prod.* **2023**, *420*, 138303.
[26] P. Bajpai, *Biermann's Handbook of Pulp and Paper: Raw Material and Pulp Making*, Elsevier, 3rd edn., **2018**, vol. 1.
[27] R. Morya, M. Kumar, I. Tyagi, A. Kumar Pandey, J. Park, T. Raj, R. Sirohi, V. Kumar, S. H. Kim, *Bioresour. Technol.* **2022**, *350*, 126916.
[28] L. Reyes, C. Nikitine, L. Vilcocq, P. Fongarland, *Green Chem.* **2020**, *22*, 8097–8115.
[29] S. Xiong, X. Li, P. Liu, S. Hao, F. Hao, Z. Yin, J. Liu, *Miner. Eng.* **2018**, *125*, 126–132.
[30] D. Hariprasad, B. Dash, M. K. Ghosh, S. Anand, *Miner. Eng.* **2007**, *20*, 1293–1295.
[31] G. Mongkhonsiri, R. Gani, P. Malakul, S. Assabumrungrat, *Comput. Chem. Eng.* **2018**, *119*, 70–84.
[32] R. C. Andeme Ela, L. Spahn, N. Safaie, R. C. Ferrier, R. G. Ong, *ACS Sustainable Chem. Eng.* **2020**, *8*, 13997–14005.
[33] M. Bonoli, V. Verardo, E. Marconi, M. F. Caboni, *J. Agric. Food Chem.* **2004**, *52*, 5195–5200.
[34] M. Pérez, I. Dominguez-López, R. M. Lamuela-Raventós, *J. Agric. Food Chem.* **2023**, *71*, 17543–17553.
[35] S. Canas, A. P. Belchoir, M. I. Spranger, R. Bruno-De-Sousa, *J. Sep. Sci.* **2003**, *26*, 496–502.
[36] P. Tomani, *Cellulose Chem. Technol.* **2010**, *44*, 53–58.
[37] A. Jinich, A. Flamholz, H. Ren, S. J. Kim, B. Sanchez-Lengeling, C. A. R. Cotton, E. Noor, A. Aspuru-Guzik, A. Bar-Even, *PLoS Comput. Biol.* **2018**, *14*, e1006471.
[38] R. Alén, in *Industrial Biorefineries and White Biotechnology*, Elsevier, **2015**, pp. 91–126.
[39] H. Kumar, R. Alén, *Sep. Purif. Technol.* **2015**, *142*, 293–298.
[40] J. Nan, D. Han, X. Zuo, *J. Power Sources* **2005**, *152*, 278–284.
[41] E. Billy, M. Joulié, R. Laucournet, A. Boulineau, E. De Vito, D. Meyer, *ACS Appl. Mater. Interfaces* **2018**, *10*, 16424–16435.
[42] K. S. Yamaguchi, D. T. Sawyer, *Isr. J. Chem.* **1985**, *25*, 164–176.
[43] J. Chivot, L. Mendoza, C. Mansour, T. Pauporté, M. Cassir, *Corros. Sci.* **2008**, *50*, 62–69.
[44] J. Partinen, P. Halli, B. P. Wilson, M. Lundström, *Miner. Eng.* **2023**, *202*, 108244.
[45] W. Xuan, A. de Souza Braga, C. Korbel, A. Chagnes, *Hydrometallurgy* **2021**, *204*, 105705.
[46] O. Bondarchuk, A. P. LaGrow, A. Kvasha, T. Thieu, E. Ayerbe, I. Urdampilleta, *Appl. Surf. Sci.* **2021**, *535*, 147699.
[47] H. Sun, K. Zhao, *J. Phys. Chem. C* **2017**, *121*, 6002–6010.
[48] C. K. Lee, K. I. Rhee, *Hydrometallurgy* **2003**, *68*, 5–10.
[49] E. Fan, J. Yang, Y. Huang, J. Lin, F. Arshad, F. Wu, L. Li, R. Chen, *ACS Appl. Energ. Mater.* **2020**, *3*, 8532–8542.
[50] E. Shinova, R. Stoyanova, E. Zhecheva, G. F. Ortiz, P. Lavela, J. L. Tirado, *Solid State Ionics* **2008**, *179*, 2198–2208.
[51] K. M. Shaju, G. V. Subba Rao, B. V. R. Chowdari, *Electrochim. Acta* **2002**, *48*, 145–151.
[52] L. Risanto, E. Hermiati, Y. Sudiyani, *Makara J. Technol.* **2014**, *18*, 67.
[53] T. Hong, J. Y. Yin, S. P. Nie, M. Y. Xie, *Food Chem X* **2021**, *12*, 100168.
[54] F. Pagnanelli, E. Moscardini, G. Granata, S. Cerbelli, L. Agosta, A. Fieramosca, L. Toro, *J. Ind. Eng. Chem.* **2014**, *20*, 3201–3207.
[55] Q. Meng, Y. Zhang, P. Dong, *Waste Manage.* **2017**, *64*, 214–218.
[56] X. Zhang, H. Cao, Y. Xie, P. Ning, H. An, H. You, F. Nawaz, *Sep. Purif. Technol.* **2015**, *150*, 186–195.
[57] M. W. Haynes, in *CRC Handbook of Chemistry and Physics*, CRC Press, 2014, 95, 80–89.
[58] A. S. Pavitt, E. J. Bylaska, P. G. Tratnyek, *Environ. Sci. Process. Impacts* **2017**, *19*, 339–349.
[59] D. M. Ritter, *J. Am. Chem. Soc.* **1947**, *69*, 46–50.
[60] E. I. Evstigneyev, S. M. Shevchenko, *Wood Sci. Technol.* **2019**, *53*, 7–47.
[61] ChemSpider | Search and share chemistry, http://www.chemspider.com/, (accessed 7 July 2023).
[62] M. L. Free, *Hydrometallurgy: Fundamentals and Applications*, Wiley (Hoboken, USA), **2014**, 1–432.
[63] K. Gu, X. Gu, Y. Wang, W. Qin, J. Han, *Green Chem.* **2023**, *25*, 4362–4374.
[64] M. K. Jha, A. Kumari, A. K. Jha, V. Kumar, J. Hait, B. D. Pandey, *Waste Manage.* **2013**, *33*, 1890–1897.
[65] Y. Ma, X. Zhou, J. Tang, X. Liu, H. Gan, J. Yang, *J. Hazard. Mater.* **2021**, *417*, 126032.
[66] F. Su, X. Zhou, X. Liu, J. Yang, J. Tang, W. Yang, Z. Li, H. Wang, Y. Ma, Y. Zhang, *J. Environ. Chem. Eng.* **2022**, *10*, 108711.
[67] C. Yang, J. Wang, P. Yang, Y. He, S. Wang, P. Zhao, H. Wang, *Sustainability* **2022**, *14*, 14169.
[68] X. Chen, C. Guo, H. Ma, J. Li, T. Zhou, L. Cao, D. Kang, *Waste Manage.* **2018**, *75*, 459–468.
[69] P. Meshram, B. D. Pandey, T. R. Mankhand, *J Chem Eng* **2015**, *281*, 418–427.
[70] A. Cipollina, D. Winter, G. Battaglia, L. Berkemeyer, J. L. Cortina, M. F. de Labastida, J. L. Rodriguez, *Ind. Eng. Chem. Res.* **2022**, *61*, 13589–13602.
[71] J. C. Ojeda Toro, I. Dobrosz-Gómez, M. Á. Gómez García, *Fluid Phase Equilib.* **2014**, *384*, 106–113.

Manuscript received: December 2, 2023
Revised manuscript received: January 17, 2024
Accepted manuscript online: February 7, 2024
Version of record online: February 23, 2024